

Current-voltage relationship in downward field-aligned current region

Alexandra P. Cran-McGreehin and Andrew N. Wright
Mathematical Institute, University of St. Andrews, St. Andrews, Fife, UK

Received 29 October 2004; revised 17 June 2005; accepted 12 July 2005; published 8 October 2005.

[1] Field-aligned electrons accelerated upward from the ionosphere to the magnetosphere are the principal charge carriers in the auroral downward field-aligned current region. Current densities, typically of the order of a few μAm^{-2} , are sustained by potential drops of several 100 V up to a few kV. This paper uses a model presented in a separate paper in this special section (Cran-McGreehin and Wright, 2005) to obtain an analytical nonlinear current-voltage relationship for the downward current, which is complimentary to the well-known linear current-voltage relation for the upward current region (Knight, 1973). Exact and approximate current-voltage relations are given. These relations are compared with FAST observations and show good agreement.

Citation: Cran-McGreehin, A. P., and A. N. Wright (2005), Current-voltage relationship in downward field-aligned current region, *J. Geophys. Res.*, 110, A10S10, doi:10.1029/2004JA010870.

1. Introduction

[2] In this paper, we study the current-voltage relation on auroral field lines carrying a downward current. We find that the B/n peak plays a crucial role in determining Ohm's Law, in particular the values of the current density (j_p) and number density (n_p) there. Other important quantities are the magnetospheric electron temperature (T), and the electron charge (e) and mass (m). We find that when the quantity $\Psi = (j_p^2 m / 2kTn_p^2 e^2)^{1/3} < 1.2$, the total potential drop along the field line is approximately

$$-\phi_m \approx \frac{3}{2} \left(\frac{j_p m^{1/2} kT}{n_p e^{5/2}} \right)^{2/3} + \frac{1}{2} \left(\frac{j_p^4 m^2 kT}{n_p^4 e^7} \right)^{1/3} + \frac{j_p^2 m}{6n_p^2 e^3} \quad (1)$$

and when $\Psi > 1.2$

$$-\phi_m \approx \frac{kT}{e} \ln \left(\frac{j_p^2 m}{n_p^2 e^2 kT} \right) + \frac{j_p^2 m}{2n_p^2 e^3} + \frac{kT}{e} \quad (2)$$

Exact expressions are also given. Our relations are compared with FAST observations, and show good agreement.

[3] Field-aligned currents form an integral part of the global magnetospheric current system, and are the means by which momentum is transferred between two different plasma environments: the hot, tenuous magnetosphere and the cold, dense ionosphere. Field-aligned currents (FACs) are known to couple other space environments, including, for example, Io and Jupiter; however, those flowing along the Earth's magnetic field lines are the easiest to observe at close range, giving vital clues as to the nature of these currents and the particle acceleration associated with them.

Several satellites and rockets, including FREJA [Marklund *et al.*, 1994] and Viking, observed occasional upward accelerated field-aligned electron beams, but it was only with the advent of the Fast Auroral SnapshoT (FAST) satellite in 1996 that it was discovered that upward electron beams occur with much the same frequency as their downward counterparts [Carlson *et al.*, 1998]. These upward beams are associated with diverging electric field structures, often located at the edge of the larger inverted V regions which support upward FACs; the improved time resolution and continuous observance of all pitch angles on FAST have been able to detect these small-scale dynamic downward current regions.

[4] Field-aligned currents are mainly carried by electrons. Observations of the downward current region by Andersson *et al.* [2002] and Ergun *et al.* [2003] have revealed complex characteristics: the potential increase occurs along a narrowly confined region of ~ 10 Debye lengths; the resulting unstable electron beam is seen along another similarly small region; and finally, the beam is stabilized by strong wave turbulence and electron phase space holes. Ion conics are also observed earthward of the potential structure, trapped between this and their mirror point. However, recent analysis has also shown examples of correlated increases in electron energy and potential, the latter of which is calculated from $\int \mathbf{E} \cdot d\mathbf{s}$ [e.g., Ergun *et al.*, 1998]. These observations suggest that the potential structures are stable at least on the electron acceleration timescale, thus lending credence to the existence of quasi-static parallel potential structures. Our model gives a simple overview of this region based on this observational evidence. Detailed studies of the downward current region have shown that upward beams occur with greatest frequency in the winter hemisphere [Elphic *et al.*, 2000], suggesting that the ion scale height and number density play a key role in determining the altitude and magnitude of the potential increase required [Cattell *et al.*, 2004].

[5] Several approaches have been employed to model the upward current region. *Knight* [1973] derived a linear current-voltage relation for the upward current region, where parallel potential drops are necessary to enable downflowing electrons to overcome magnetic mirror forces to carry the current. More recent models include *Rönmark* [2002], *Vedin and Rönmark* [2004] and *Wright and Hood* [2003]. Relatively little attention, however, has focused on the electron dynamics of the downward current region. It was thought that no significant potential would be required here, as the ionosphere is a plentiful source of electrons; however, the falling ion number density restricts the electron beam's number density as it flows upward in such a way that it must be accelerated at a particular critical altitude in order to carry the required current. *Temerin and Carlson* [1998] use an electron fluid model with fixed ion density, invoking quasi-neutrality to calculate the required parallel potential drop. They obtain parallel potential drops of several kV for current densities of a few μAm^{-2} . *Jasperse* [1998] presents a Vlasov model including ion heating and wave effects, which explains the production of upward field-aligned electron beams and ion conics.

[6] In this paper, we analyze the downward current model presented in a separate paper in this special section [*Cran-McGreehin and Wright*, 2005, hereinafter referred to as paper 1], which builds on the *Temerin and Carlson* [1998] model by using electron distribution functions and modeling the entire F region. Mathematical analysis of this downward current model leads to a single current-voltage relation which can be simplified to give two nonlinear approximations valid under different regimes of the downward current region.

2. Model

[7] In this paper, we present results obtained from the model in paper 1. This is a one-dimensional Vlasov model of an upward accelerated electron beam along an auroral field line, extending from the base of the F region, ℓ_m , taken to be at a radial distance of $1 R_E$, to a distant point in the magnetosphere, ℓ_0 . We model the magnetic field as being locally dipolar in the acceleration region, giving a magnetic field strength of

$$B = B_0 \frac{\sqrt{1 + 3 \sin^2 \theta}}{\cos^6 \theta} \quad (3)$$

where B_0 is a constant, θ is the latitude and

$$r = LR_E \cos^2 \theta \quad (4)$$

where we take $L = 10$ to give a typical auroral field line. The arc length element along \mathbf{B} , $d\ell$, is given by

$$d\ell = d\theta \sqrt{r^2 + \left(\frac{dr}{d\theta}\right)^2} \quad (5)$$

[8] Using equations (4) and (5), the length along the field line, ℓ , which increases as you enter the ionosphere, is found to be

$$\ell = \int_0^\theta LR_E \cos \theta \sqrt{1 + 3 \sin^2 \theta} \quad (6)$$

which can be solved to give

$$\ell = \frac{LR_E}{2\sqrt{3}} \left(\frac{1}{2} \sinh \left(2 \sinh^{-1} \left(\sqrt{3} \sin \theta \right) \right) + \sinh^{-1} \left(\sqrt{3} \sin \theta \right) \right) \quad (7)$$

[9] The ion number density is considered to be fixed in time, and has an exponentially decaying profile

$$n = n_0 + (n_m - n_0) \exp \left(-\frac{(r - R_E)}{h} \right) \quad (8)$$

where the ion number densities at ℓ_m and ℓ_0 are n_m and n_0 , respectively, and the scale height h ranges from 50 to a few hundred km. The scale height could simply represent the gravitational stratification of the ions, or could be increased in the case of strong ion conics to represent redistribution of ions by the mirror force [e.g., *Jasperse*, 1998]. A top-hat ionospheric electron distribution is defined at ℓ_m , and a Maxwellian magnetospheric electron population at ℓ_0 . Most of the ionospheric electrons are trapped by a small ambipolar electric field, but the most energetic ones escape and are accelerated into the magnetosphere to form the beam. We define ℓ_c to be the point earthward of which all ionospheric electrons except those forming the beam are trapped. This location is important in the mathematical analysis and is where different solutions must be matched. For the purposes of this paper we define the ‘‘ionosphere’’ and ‘‘magnetosphere’’ in terms of this location: the ionosphere extends from ℓ_m , the base of the F region, to ℓ_c , and the magnetosphere is between ℓ_c and ℓ_0 . The location of ℓ_c , along with other significant locations in the model, are shown schematically in Figure 1. The lower boundary of the model by *Temerin and Carlson* [1998] is at ℓ_c , where they input appropriate boundary conditions obtained from data. Our lower boundary is the base of the F region, ℓ_m , and the location of ℓ_c , where the electron beam emerges into the magnetosphere, is determined self-consistently from the model parameters (see paper 1). In paper 1, we reproduced *Temerin and Carlson's* [1998] result for a specific example (see their Figure 1) by mapping their boundary conditions at ℓ_c to ℓ_m . This reproduced their solution exactly, and gives confidence that our extended calculation is correct.

[10] A full derivation of the equations is given in paper 1, to which the reader is referred for full details. Here, we outline the main features. The system is solved by using Liouville's theorem and the current continuity condition, $\nabla \cdot \mathbf{j} = 0$, which reduces to

$$\frac{j(\ell)}{B(\ell)} = \frac{j_m}{B_m} \quad (9)$$

where j_m and B_m are the values of the current density and magnetic field strength at ℓ_m . Expressions for the electron number density in the ionosphere and magnetosphere are obtained, and quasineutrality is then invoked to yield dimensionless equations. These contain three dimensionless parameters: a normalized current density, α , which is positive for downward currents, given by

$$\alpha = \frac{j_m}{n_m e a_m} \quad (10)$$

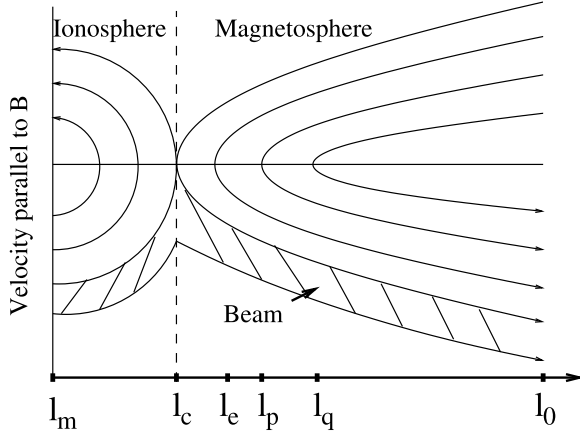


Figure 1. Diagram showing the three electron populations: mirroring magnetospheric electrons, trapped ionospheric electrons, and the beam. This diagram is not to scale: The magnetospheric electron population is much more energetic (~ 1 keV) than that in the ionosphere (~ 1 eV). Key locations derived from the model are l_m , the base of the F region; l_c , the ionospheric trapping point; l_e , the point where E_{\parallel} maximizes; l_p , the location of the B/n peak; l_q , the stationary point described in section 3; and l_0 , a distant reference point in the magnetosphere.

where a_m is the ionospheric electron distribution thermal velocity width; η , the ratio of the ionospheric and magnetospheric temperatures, given by

$$\eta = \frac{ma_m^2}{2kT} \quad (11)$$

where kT is the thermal energy of the magnetospheric electron population; and a normalized electric potential difference, $\Delta\tilde{\Phi}(\ell)$, relative to that at l_m , given by

$$\Delta\tilde{\Phi} = \frac{2e}{ma_m^2}(\phi - \phi_m) \quad (12)$$

where ϕ_m is the potential at l_m , and $\phi(l_0) = 0$. The ionospheric and magnetospheric equations are shown below:

$$\frac{n(\ell)}{B(\ell)} \Big/ \frac{n_0}{B_0} = A \left(\sqrt{(1+2\alpha)^2 + \Delta\tilde{\Phi}} + \sqrt{1 + \Delta\tilde{\Phi}} \right) \quad (13)$$

$$\frac{n(\ell)}{B(\ell)} \Big/ \frac{n_0}{B_0} = A \left(\sqrt{(1+2\alpha)^2 + \Delta\tilde{\Phi}} - \sqrt{1 + \Delta\tilde{\Phi}} \right) + \frac{B_0}{B(\ell)}(1 - AC) \exp(\eta(\Delta\tilde{\Phi} + \tilde{\Phi}_m)), \quad (14)$$

where

$$A = \left(\frac{n_m}{n_0} \right) \left(\frac{B_0}{B_m} \right) \frac{1}{2(1+\alpha)}. \quad (15)$$

and

$$C = \sqrt{(1+2\alpha)^2 - \tilde{\Phi}_m} - \sqrt{1 - \tilde{\Phi}_m} \quad (16)$$

[11] In the magnetospheric equation (14), the first term on the right hand side corresponds to the number density contribution from the electron beam, while the second term gives the contribution from the mirroring Maxwellian magnetospheric electron population. $\tilde{\Phi}_m = 2e\phi_m/(ma_m^2)$ in equations (14) and (16) corresponds to the total change in potential along the field line, since using equation (12), $\Delta\tilde{\Phi}(l_m) = 0$ and $\Delta\tilde{\Phi}(l_0) = -\tilde{\Phi}_m$. For downward currents, $\tilde{\Phi}_m$ is negative, so the total potential increase along the field line is given by $-\tilde{\Phi}_m$. Following *Temerin and Carlson* [1998] we have neglected the magnetospheric Maxwellian electron number density in the ionosphere (equation (13)) compared to the ionospheric electron number density. Paper 1 confirmed that this is a good approximation. If an additional term representing magnetospheric electrons was added to the RHS of equation (13), this would typically increase the relative electron number density by 10^{-4} – 10^{-8} , and as suggested by *Temerin and Carlson* [1998] would have no significant effect on our solution. Indeed, we used the methods of paper 1 to find the exact numerical solution to (13) and (14) for standard parameters, with and without the inclusion of magnetospheric electrons in (13). This changed the altitude of l_c by 0.003% and $\tilde{\Phi}_m$ by 0.06%, confirming the suitability of equation (13).

[12] In paper 1, we solve equations (13) and (14) numerically at each point along the field line to give a potential curve, in a similar fashion to *Temerin and Carlson* [1998]. In the ionosphere, we find that $\Delta\tilde{\Phi}$ decreases from 0 to -1 between l_m and l_c ; this forms the ambipolar electric field which traps most of the ionospheric electron population close to the Earth. The most energetic electrons, although decelerated by this ambipolar potential, manage to penetrate into the magnetosphere to form the upgoing current-carrying electrons. Beyond l_c , the potential increases monotonically, and the parallel electric field maximizes at l_e , between l_c and the B/n peak (see Figure 1). This kickstarts the electron beam acceleration, most of which occurs in a small acceleration region of width ~ 1000 km. Qualitatively, results from paper 1 show that as the current density increases, so does $|\tilde{\Phi}_m|$, the potential increase required to accelerate the beam; $|\tilde{\Phi}_m|$ also increases as the difference in electron ionospheric and magnetospheric temperatures increases, which corresponds to a decrease in η .

3. Stationary Point Analysis

3.1. Magnetospheric Roots

[13] We know the value of n/B along the field line from equations (3) and (8), so in the ionosphere, we can solve equation (13) at each point between l_m and l_c to find the potential, $\Delta\tilde{\Phi}(\ell)$. Solving equation (14) to find the potential variation in the magnetosphere is not so straightforward, as the equation contains a free parameter $\tilde{\Phi}_m$, where $\Delta\tilde{\Phi}(l_0) = -\tilde{\Phi}_m$. Varying this parameter produces a family of curves of the roots of $\Delta\tilde{\Phi}$ in equation (14); *Temerin and Carlson* [1998] also noted the multivalued nature of their solution.

[14] In general, the solutions to this equation are described by two branches, or curves, for a given $\tilde{\Phi}_m$, as shown in Figure 2. For one particular critical value of $\tilde{\Phi}_m$, these branches touch at a stationary point. If we take $|\tilde{\Phi}_m| <$ critical $|\tilde{\Phi}_m|$, then there are two branches, one to the right of

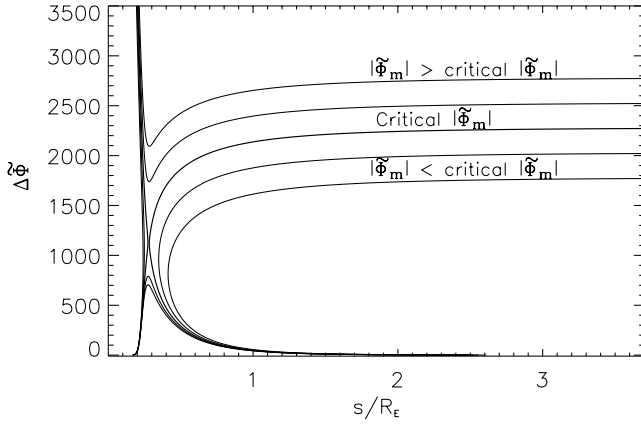


Figure 2. Plot showing the form of the two roots of magnetospheric equation (14) for different values of the parameter $\tilde{\Phi}_m$, where $\alpha = 5 \times 10^{-5}$, $\eta = 10^{-3}$ and $s = \ell - \ell_m$. If $|\tilde{\Phi}_m|$ is larger than the critical value, then upper and lower branches of $\Delta\tilde{\Phi}$ exist all the way along the field line (above and below the x point), but do not meet at any point, and neither curve satisfies our boundary conditions. If $|\tilde{\Phi}_m|$ is smaller than the critical value, then there are again two branches of $\Delta\tilde{\Phi}$, one to the right and the other to the left of the x point. Thus there are points along the field line between these two curves for which no root of $\Delta\tilde{\Phi}$ exists. All of these curves are unphysical, but there is a unique critical value of $\tilde{\Phi}_m$ for which the two curves of $\Delta\tilde{\Phi}$ meet at a stationary x point. The solution which satisfies our boundary conditions is the monotonically increasing one, which switches from the lower to the upper branch as it passes through the x point.

the x point, and another to the left. Clearly, there are points along the field line between these two curves for which no root exists, so we exclude these values of $\tilde{\Phi}_m$ as being unphysical. On taking $|\tilde{\Phi}_m| > \text{critical } |\tilde{\Phi}_m|$, we again find two branches, this time above and below the x point. Both of these curves are continuous: however, we assume in the derivation of equation (14) that the Maxwellian electron distribution at ℓ_0 remains Maxwellian throughout the magnetosphere. This is only the case for a monotonically decreasing potential from the magnetospheric end, since any increase will lead to a hole in phase space around $v_{\parallel} = 0$, giving a non-Maxwellian distribution. Thus these curves are mathematical roots of equation (14), but this equation no longer describes our system accurately, and so these curves must be discounted. Thus we choose the monotonically increasing continuous curve which passes through the stationary point as the physically relevant solution for this problem. Numerically, we search for the value of $\tilde{\Phi}_m$ for which the solutions touch at a stationary point we label ℓ_q , and choose the lower solution earthward of ℓ_q , and the upper solution beyond ℓ_q . This gives a systematic way of producing Temerin and Carlson type solutions.

3.2. Stationary Point Equations

[15] In paper 1 we showed numerically that the B/n peak determined the solution; altering the ion number density on either side of the peak resulted in no difference to $\tilde{\Phi}_m$. We now understand why this is. The stationary point outlined

above can be described mathematically. To do this, we make a small simplification to equation (14) to allow solution of the resulting equations, by using the approximation

$$\sqrt{(1+2\alpha)^2 + \Delta\tilde{\Phi}} - \sqrt{1 + \Delta\tilde{\Phi}} \approx \frac{2\alpha(1+\alpha)}{\sqrt{1 + \Delta\tilde{\Phi}}} \quad (17)$$

valid when $1 + \Delta\tilde{\Phi} \gg 4\alpha(\alpha + 1)$. Since $\alpha \ll 1$, typically $\sim 10^{-5} - 10^{-3}$, and our stationary point ℓ_q lies in the middle of the acceleration region where $\Delta\tilde{\Phi}$ is large, this is an excellent approximation. Indeed, for typical parameters, $4\alpha(\alpha + 1)/(1 + \Delta\tilde{\Phi}) \sim 10^{-7} - 10^{-6}$. From this approximation, we obtain

$$\begin{aligned} \frac{n(\ell)}{B(\ell)} / \frac{n_0}{B_0} &= \left(\frac{n_m}{n_0}\right) \left(\frac{B_0}{B_m}\right) \frac{\alpha}{\sqrt{1 + \Delta\tilde{\Phi}}} \\ &+ \frac{B_0}{B(\ell)} (1 - AC) \exp(\eta(\Delta\tilde{\Phi} + \tilde{\Phi}_m)) \end{aligned} \quad (18)$$

[16] Evaluating this relation at the stationary point, ℓ_q , where $n(\ell) = n_q$, $B(\ell) = B_q$ and $\Delta\tilde{\Phi} = \Delta\tilde{\Phi}_q$, we obtain our first stationary point equation

$$\begin{aligned} \frac{n_q}{n_0} &= \left(\frac{n_m}{n_0}\right) \left(\frac{B_q}{B_m}\right) \frac{\alpha}{\sqrt{1 + \Delta\tilde{\Phi}_q}} \\ &+ (1 - AC) \exp(\eta(\Delta\tilde{\Phi}_q + \tilde{\Phi}_m)) \end{aligned} \quad (19)$$

[17] The stationary point at ℓ_q is a standard two-variable saddle point. At a stationary point of a general function $g(x, y)$, $\partial g/\partial x = \partial g/\partial y = 0$ [see *Salas et al.*, 2003, chapter 15]. Equation (18) tells us that $G(B, \Delta\tilde{\Phi}, \tilde{\Phi}_m) = 0$, where n is a known function of B and all other parameters are given, but $\tilde{\Phi}_m$ is not (hence it is retained as a variable). Setting $G = 0$ implicitly defines $\tilde{\Phi}_m$ given B and $\Delta\tilde{\Phi}$, which we can express as $\tilde{\Phi}_m = g(B, \Delta\tilde{\Phi})$. We see how B and $\Delta\tilde{\Phi}$ play the roles of x and y in a textbook two-variable stationary point analysis. Indeed, the contours of $\tilde{\Phi}_m$ in Figure 2 were calculated from just this expression (except it uses s rather than B as the field-aligned coordinate). The requirements $\partial g/\partial x = \partial g/\partial y = 0$ become $(\partial g/\partial B)_{\Delta\tilde{\Phi}} = \partial g/\partial B + (\partial g/\partial n)(dn/dB) = 0$ and $(\partial g/\partial \Delta\tilde{\Phi})_B = 0$ at ℓ_q , giving us two more equations for the stationary point:

$$\begin{aligned} 0 &= -\frac{1}{2} \left(\frac{n_m}{n_0}\right) \left(\frac{B_q}{B_m}\right) \frac{\alpha}{(1 + \Delta\tilde{\Phi}_q)^{\frac{3}{2}}} \\ &+ \eta(1 - AC) \exp(\eta(\Delta\tilde{\Phi}_q + \tilde{\Phi}_m)) \end{aligned} \quad (20)$$

$$B_0 \frac{d}{dB} \left(\frac{n(B)}{n_0}\right)_q - \left(\frac{n_m}{n_0}\right) \left(\frac{B_0}{B_m}\right) \frac{\alpha}{\sqrt{1 + \Delta\tilde{\Phi}_q}} = 0 \quad (21)$$

[18] Thus we have three equations at the stationary point ((19), (20), and (21)), and four unknowns (n_q , B_q , $\Delta\tilde{\Phi}_q$, and $\tilde{\Phi}_m$). In principle, we could solve this system of equations by introducing a fourth equation relating n_q and B_q . However, this proves to be unnecessary, as we shall show in section 4 that it is possible to get good estimates of n_q and B_q by another route. We do not use equation (21) in our derivation of an analytical expression for $\tilde{\Phi}_m$, but we have included it for completeness, since it would be necessary to use it if n_q and B_q were unknown.

Substituting for the exponential in equation (19) using equation (20) we obtain

$$\frac{n_q}{n_0} = \frac{n_m}{n_0} \frac{B_q}{B_m} \frac{\alpha}{\sqrt{1 + \Delta\tilde{\Phi}_q}} + \frac{\alpha}{2\eta} \frac{n_m}{n_0} \frac{B_q}{B_m} (1 + \Delta\tilde{\Phi}_q)^{-3/2} \quad (22)$$

[19] This can be rearranged to give the cubic

$$X^3 - \alpha c_q X^2 - \frac{\alpha c_q}{2\eta} = 0 \quad (23)$$

where $X = \sqrt{1 + \Delta\tilde{\Phi}_q}$ and $c_q = (n_m/n_q)(B_q/B_m)$.

3.3. Solving the Cubic

[20] The cubic equation (23) can be solved by first transforming it:

$$\begin{aligned} X^3 - \alpha c_q X^2 - \frac{\alpha c_q}{2\eta} &= \left(X - \frac{\alpha c_q}{3}\right)^3 - \frac{\alpha^2 c_q^2}{3} \left(X - \frac{\alpha c_q}{3}\right) \\ &\quad - \left(\frac{\alpha c_q}{2\eta} + \frac{2\alpha^3 c_q^3}{27}\right) \end{aligned} \quad (24)$$

[21] Now we can use the fact that a cubic of the form $Y^3 + pY + q = 0$ has a real solution $Y = s - t$, where $p = 3st$ and $q = t^3 - s^3$. In the case of equation (24), $Y = X - (\alpha c_q/3)$, and this gives

$$\begin{aligned} \sqrt{1 + \Delta\tilde{\Phi}_q} &= \sqrt[3]{\frac{\alpha c_q}{4\eta} + \frac{\alpha^3 c_q^3}{27} - \frac{\alpha c_q}{4\eta} \sqrt{1 + \frac{8\eta\alpha^2 c_q^2}{27}}} \\ &\quad + \sqrt[3]{\frac{\alpha c_q}{4\eta} + \frac{\alpha^3 c_q^3}{27} + \frac{\alpha c_q}{4\eta} \sqrt{1 + \frac{8\eta\alpha^2 c_q^2}{27}}} \\ &\quad + \frac{\alpha c_q}{3} \end{aligned} \quad (25)$$

[22] We are now in a position to derive an expression for $\tilde{\Phi}_m(\alpha, \eta, n_q, B_q)$ by rearranging equation (20) to give

$$\tilde{\Phi}_m = \frac{1}{\eta} \ln \left[\frac{\alpha}{2\eta} \frac{n_m}{n_0} \frac{B_q}{B_m} (1 - AC)^{-1} (1 + \Delta\tilde{\Phi}_q)^{-3/2} \right] - \Delta\tilde{\Phi}_q \quad (26)$$

[23] We can now substitute equation (25) into equation (26) to obtain

$$\begin{aligned} \tilde{\Phi}_m &= \frac{1}{\eta} \ln \left(\frac{2n_q}{n_0(1 - AC)} \right) - \frac{3}{\eta} \ln[y(\Psi)] \\ &\quad - \left(\frac{\alpha c_q}{4\eta} \right)^{2/3} [y(\Psi)]^2 + 1 \end{aligned} \quad (27)$$

where

$$\begin{aligned} y(\Psi) &= \sqrt[3]{1 + \frac{4\Psi^3}{27} - \sqrt{1 + \frac{8\Psi^3}{27}}} \\ &\quad + \sqrt[3]{1 + \frac{4\Psi^3}{27} + \sqrt{1 + \frac{8\Psi^3}{27}}} + \frac{4^{1/3}}{3} \Psi \end{aligned} \quad (28)$$

and

$$\Psi = \alpha^{2/3} c_q^{2/3} \eta^{1/3} \quad (29)$$

[24] The constant C , contained in our expression for $\tilde{\Phi}_m$ in equation (27) and defined in equation (16), depends on $\tilde{\Phi}_m$. However, we can split up the first term on the RHS of equation (27) as follows:

$$\frac{1}{\eta} \ln \left(\frac{2n_q}{n_0(1 - AC)} \right) = \frac{1}{\eta} \ln \left(2 \frac{n_q}{n_0} \right) - \frac{1}{\eta} \ln(1 - AC) \quad (30)$$

where typically, $\eta^{-1} \ln(1 - AC)/\tilde{\Phi}_m \sim 10^{-4}$. Thus we can safely neglect this term to obtain a more useful expression for $\tilde{\Phi}_m$:

$$\begin{aligned} \tilde{\Phi}_m &= \frac{1}{\eta} \ln \left(2 \frac{n_q}{n_0} \right) - \frac{3}{\eta} \ln[y(\Psi)] \\ &\quad - \left(\frac{\alpha c_q}{4\eta} \right)^{2/3} [y(\Psi)]^2 + 1 \end{aligned} \quad (31)$$

[25] When $\tilde{\Phi}_m$ is evaluated using equation (31) and the exact value of ℓ_q , taken from a numerical solution, we find exact agreement with the numerically derived value of $\tilde{\Phi}_m$, as expected. The results of such exact calculations for a range of values of α and η are displayed in Figure 3. The expression in equation (31) is helpful because although $\tilde{\Phi}_m$ is a function of two variables, α and η , the expression contains $y(\Psi)$, a function of one variable which is easier to expand in a Taylor series to simplify the expression.

4. Taylor Series Approximations

4.1. Approximation of ℓ_q

[26] It is very hard to pinpoint the exact location of ℓ_q analytically by solving the stationary point equations. However, the numerical solutions of paper 1 can be used to show that ℓ_q always lies very close to the B/n peak. The results of these numerical solutions are shown in Figure 4 for varying ion scale heights (h), current densities and electron temperatures. The ion scale height varies with ion temperature, which can range from 10^3 K to a few thousand K: this gives ion scale heights from 50 to a few hundred km. The values of the two small parameters, α and η , do have a small effect on the location of ℓ_q : as α (the normalized current density) increases, ℓ_q moves closer to the B/n peak; and as the ratio of ionospheric and magnetospheric electron temperatures, η , increases (implying a lower magnetospheric temperature), ℓ_q again moves closer to the B/n peak. However, in all applicable cases, the difference in height is no more than 10%. As a result of this, we can make the approximations $n_q \approx n_p$ and $B_q \approx B_p$ in the analytical solution, and obtain a very accurate approximation to $\tilde{\Phi}_m$. Thus we can approximate the exact solution by replacing c_q in equation (29) with

$$c_p = \left(\frac{n_m}{n_p} \right) \left(\frac{B_p}{B_m} \right) \quad (32)$$

[27] Figure 4 shows a linear relationship between the B/n location and ion scale height, h . This work illustrates that, not surprisingly, the ion scale height plays the major role in determining the position of the B/n peak, and hence of ℓ_q . This agrees with work on the prevalence of beams in the

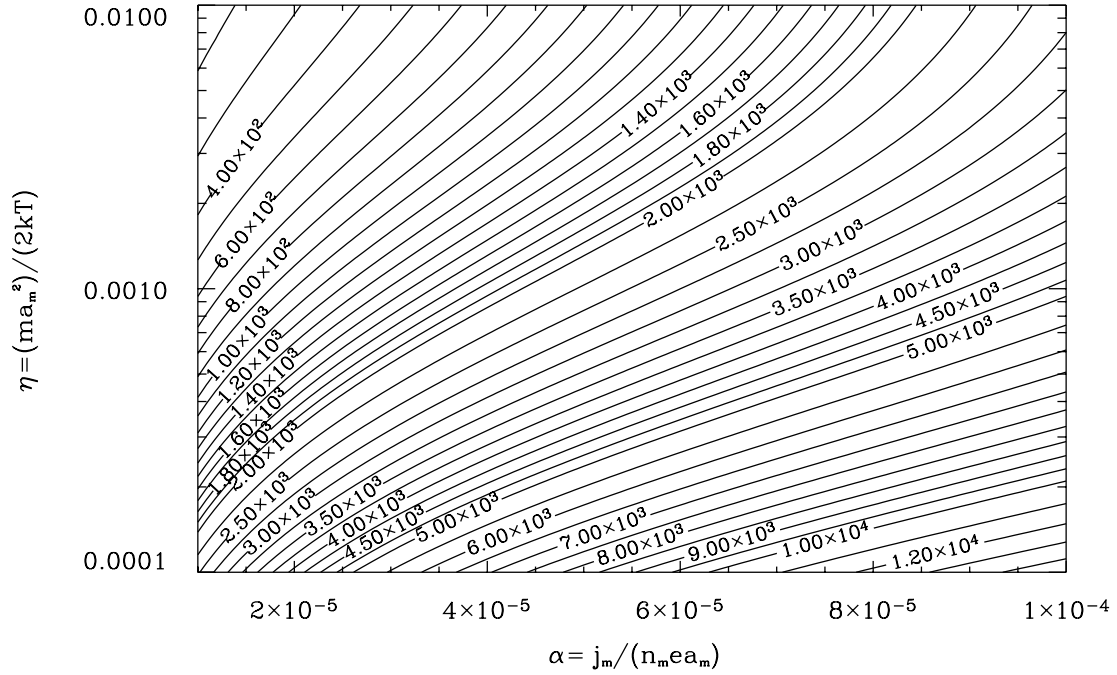


Figure 3. Contour plot of analytical solution of $\tilde{\Phi}_m$, the total potential increase along the field line given by equation (31). Parameters used are $n_m/n_0 = 10^6$, $h = 100$ km and an ionospheric temperature of 1 eV. This shows that the potential increases with increasing current density and magnetospheric temperature. Generally, potentials are of the order of ~ 100 V to ~ 1 kV.

winter auroral region [Carlson *et al.*, 1998; Cattell *et al.*, 2004], which indicate the important role played by the scale height and number density.

4.2. Taylor Series

[28] Equation (31) constitutes an analytical solution of $\tilde{\Phi}_m$, the total normalized potential increase along the field line, in terms of α , η , c_q and n_q . However, it is a cumbersome expression, and it would be very helpful to

obtain more user-friendly approximations for use in future analytical work. This can be achieved by performing a Taylor series expansion on $\gamma(\Psi)$, given in equation (28), and then substituting this expansion into equation (31) to obtain an approximate relation.

4.2.1. $\Psi \ll 1$

[29] First, we assume that $\Psi = \alpha^{2/3} c_p^{2/3} \eta^{1/3}$ is small. This corresponds to cases where α and η are both small, implying small current densities and moderate to high

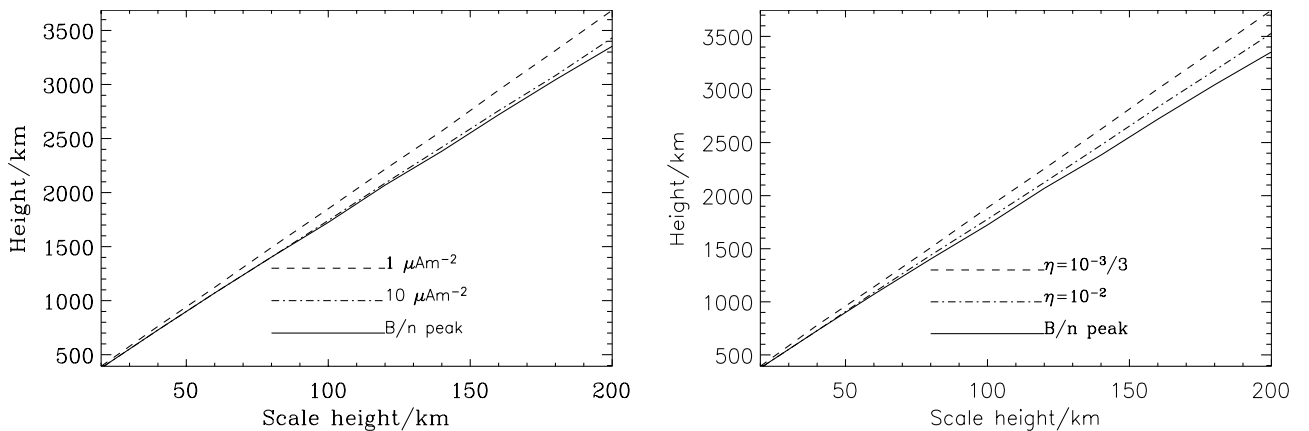


Figure 4. Location of ℓ_q (the stationary point, dashed and dot-dashed lines) and ℓ_p (the B/n peak, solid line) plotted against ion scale height for different values of (left) α and (right) η . In Figure 4 (left), η is taken to be 10^{-3} , which corresponds, for example, to ionospheric and magnetospheric electron temperatures of 1 eV and 1 keV, respectively. In Figure 4 (right), α is fixed at 1×10^{-5} , corresponding to a downward current density at ℓ_m of $1 \mu\text{Am}^{-2}$. The fact that ℓ_q is always close to the B/n peak is shown, so we can make the assumption that $n_q \approx n_p$ and $B_q \approx B_p$ in our analytical solution.

Table 1. Values of the Constant c_p for Different Ion Number Densities (n_m/n_0) and Scale Heights (h)^a

	5×10^4	7.5×10^4	1.0×10^5	2.5×10^5	5.0×10^5	7.5×10^5	1.0×10^6
50 km	3.514×10^4	5.225×10^4	6.924×10^4	1.697×10^5	3.346×10^5	4.976×10^5	6.595×10^5
100 km	2.621×10^4	3.870×10^4	5.103×10^4	1.231×10^5	2.398×10^5	3.542×10^5	4.671×10^5
150 km	2.019×10^4	2.963×10^4	3.890×10^4	9.261×10^4	1.786×10^5	2.623×10^5	3.446×10^5
200 km	1.593×10^4	2.325×10^4	3.041×10^4	7.158×10^4	1.369×10^5	2.000×10^5	2.619×10^5
250 km	1.281×10^4	1.861×10^4	2.426×10^4	5.653×10^4	1.073×10^5	1.562×10^5	2.039×10^5
300 km	1.046×10^4	1.513×10^4	1.967×10^4	4.544×10^4	8.571×10^4	1.243×10^5	1.619×10^5

^aThe first row shows values of n_m/n_0 , and the first column gives different values of h .

magnetospheric temperatures. Performing a Taylor expansion of equation (28) around $\Psi = 0$ gives us

$$y(\Psi) = 2^{1/3} + \frac{4^{1/3}}{3}\Psi + \frac{2}{9}\Psi^2 + \frac{4}{81}2^{1/3}\Psi^3 + O(\Psi^4) \quad (33)$$

[30] Substituting this back into equation (31) and using equation (29) with $c_q \approx c_p$, we obtain the following expression for $\tilde{\Phi}_m$

$$\begin{aligned} \tilde{\Phi}_m(\alpha, \eta) \approx & \frac{1}{\eta} \ln\left(\frac{n_p}{n_0}\right) - 3\left(\frac{\alpha c_p}{2\eta}\right)^{\frac{2}{3}} - \frac{1}{2^{1/3}} \left(\frac{\alpha^{4/3} c_p^{4/3}}{\eta^{1/3}}\right) \\ & - \frac{\alpha^2 c_p^2}{3} + O\left(\alpha^{8/3} c_p^{8/3} \eta^{1/3}\right) \end{aligned} \quad (34)$$

[31] It is possible to neglect the first term on the right hand side, since $n_p \approx n_0$. Thus, noting that α is positive for downward currents, the expansion can be simplified to

$$-\tilde{\Phi}_m \approx 3\left(\frac{\alpha c_p}{2\eta}\right)^{\frac{2}{3}} + \frac{1}{2^{1/3}} \left(\frac{\alpha^{4/3} c_p^{4/3}}{\eta^{1/3}}\right) + \frac{\alpha^2 c_p^2}{3} \quad (35)$$

4.2.2. $\Psi \gg 1$

[32] The other possibility is that $\Psi = \alpha^{2/3} c_p^{2/3} \eta^{1/3}$ is large. This implies large values of α and η , i.e., large current densities and low magnetospheric temperatures. Performing a Taylor expansion of equation (28) about $\Psi = \infty$ is equivalent to expanding $y(1/\Psi)$ about $1/\Psi = 0$. So, letting $a = 1/\Psi$, we can manipulate equation (28) to obtain

$$\begin{aligned} Y(a) = & \left(\frac{1}{a}\right) \left(\sqrt[3]{\frac{4}{27} + a^3} - \sqrt{\frac{8}{27} a^{3/2}} \sqrt{1 + \frac{27}{8} a^3} \right. \\ & \left. + \sqrt[3]{\frac{4}{27} + a^3} + \sqrt{\frac{8}{27} a^{3/2}} \sqrt{1 + \frac{27}{8} a^3} + \frac{4^{1/3}}{3} \right) \end{aligned} \quad (36)$$

[33] Expanding the bracket around $a = 0$ yields

$$aY(a) = 4^{1/3} + \frac{a^3}{2^{1/3}} + O(a^4) \quad (37)$$

which can be translated to

$$y(\Psi) = 4^{1/3}\Psi + \frac{1}{2^{1/3}\Psi^2} + O(\Psi^{-3}) \quad (38)$$

[34] As above, we can substitute this into equation (31) to obtain

$$\begin{aligned} \tilde{\Phi}_m(\alpha, \eta) \approx & \frac{1}{\eta} \ln\left(\frac{2n_p}{n_0}\right) - \frac{1}{\eta} \ln\left(4\alpha^2 c_p^2 \eta\right) - \alpha^2 c_p^2 \\ & - \frac{1}{\eta} + 1 + O\left(\alpha^{-2/3} c_p^{-2/3} \eta^{-4/3}\right) \end{aligned} \quad (39)$$

[35] For the same reasons as in the first case, we can simplify the first term to $\eta^{-1} \ln(2)$ to obtain the following approximation

$$-\tilde{\Phi}_m \approx \frac{1}{\eta} \ln\left(2\alpha^2 c_p^2 \eta\right) + \alpha^2 c_p^2 + \frac{1}{\eta} \quad (40)$$

4.3. Accuracy of Approximations

[36] Equations (31), (28) and (29) give the analytical form of $\tilde{\Phi}_m$ if c_q is known. However, finding this parameter is awkward and involves numerical work, since the location of ℓ_q changes with α and η for a given equilibrium model. If we let $c_q \approx c_p$, which is easier to calculate (a range of values are given in Table 1), we obtain approximate relations for $\tilde{\Phi}_m$ which are easy to use.

[37] The relative accuracy of the two approximations is shown in Figure 5 for two different values of η . In each case, $\Psi < 1$ for small current densities and the first approximation in equation (35) is accurate. Many relevant scenarios in the downward current region with low to moderate current densities and average ionospheric and magnetospheric electron temperatures satisfy $\Psi \ll 1$, so this approximation is valid. Even as α increases and Ψ approaches 1 and exceeds it, this approximation remains very accurate. Then, at some value of $\Psi \sim 1$, the first approximation loses accuracy as we enter a different regime where the second approximation in equation (40) should be adopted. In all cases for the standard parameters we have chosen, the appropriate approximation is valid to within 6.4% of the exact potential increase.

4.4. An Example

[38] In order to estimate the potential increase for a given event in the downward current region, the following steps should be carried out.

[39] Step 1 is to choose the parameters for the equilibrium model: the magnetospheric thermal electron energy (kT), the ionospheric electron thermal energy ($m_e a_m^2/2$), the ion number density at the base of the F region (n_m) and at ℓ_0 in the magnetosphere (n_0), the ion scale height (h), and the current density at the base of the F region (j_m). From these, calculate

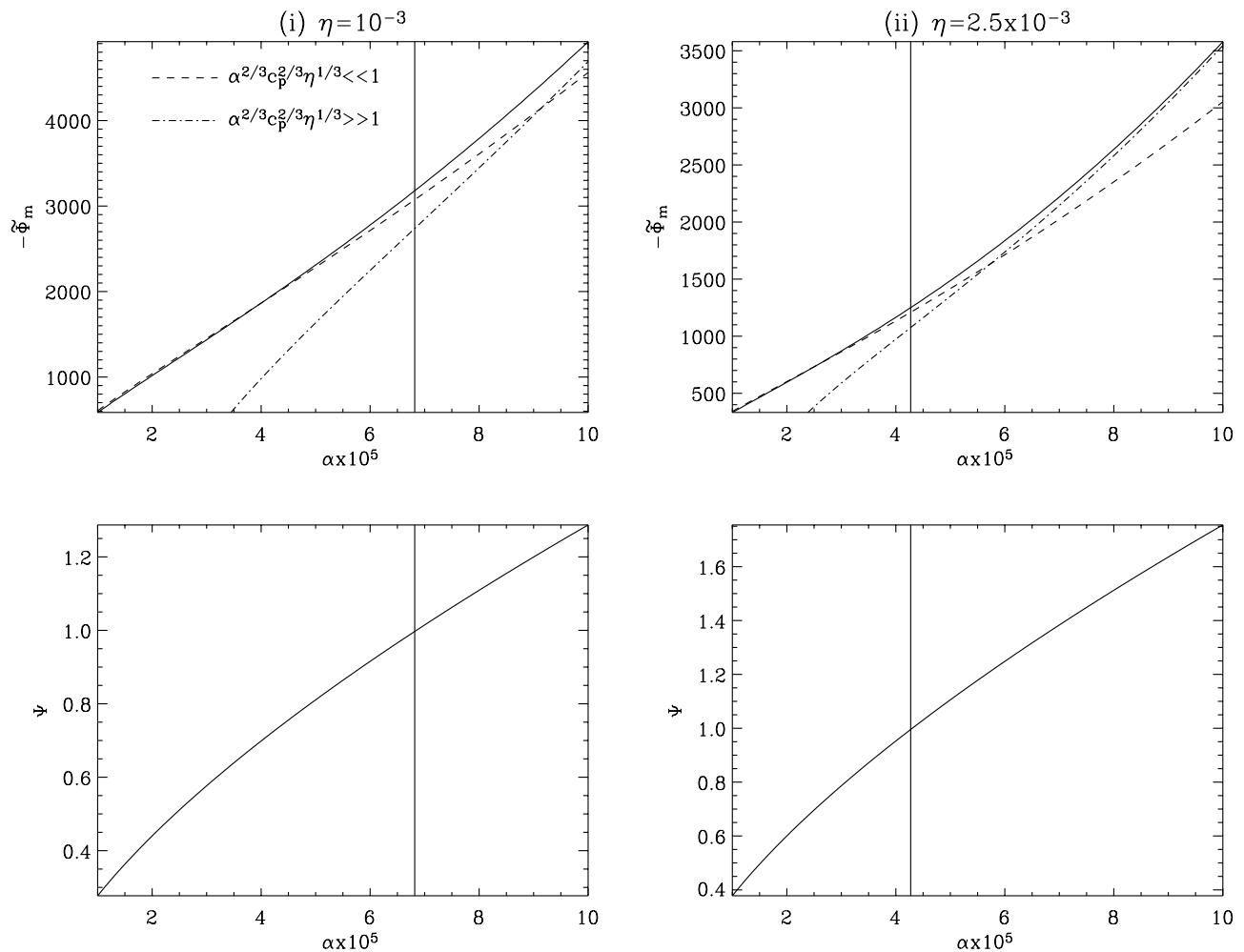


Figure 5. Graphs showing the regions of validity of the two Taylor expansions. The current densities run from 1 to 10 μAm^{-2} ; for an ionospheric electron temperature of 1 eV, η values of 10^{-3} and 2.5×10^{-3} correspond to magnetospheric electron temperatures of 1 keV and 400 eV, respectively. (top) The solid line represents the actual values of $\tilde{\Phi}_m$ found by solving equation (14) numerically, or using the numerically determined values of n_q and B_q in equation (31). The dashed line shows the approximation given in equation (35), which is most accurate for small α and η , while the dot-dashed line shows the approximation given in equation (40), most accurate for larger values of α and η . (bottom) The corresponding values of Ψ are plotted, defined in equation (29), which is the variable in which we derive the Taylor series. The vertical solid line indicates the point at which $\Psi = 1$ in each case. The first approximation is more accurate for $\Psi \leq 1.2$. When $\Psi \geq 1.2$, the second approximation should be adopted.

the dimensionless parameters α and η , from equations (10) and (11), respectively.

[40] Step 2 is to determine the parameter c_p given in equation (32). This can be done by using Table 1. Also determine the value of Ψ in equation (29), replacing c_q with c_p .

[41] Step 3 contains two options. The first is to use equation (28) to determine $y(\Psi)$ and substitute into equation (31), using $n_q \approx n_0$ and $c_q \approx c_p$ to obtain $\tilde{\Phi}_m$. The second is to use the approximation in equation (35) if $\Psi < 1$, or the one in equation (40) if $\Psi > 1$. Note that $\tilde{\Phi}_m$ is negative for downward currents, and $-\tilde{\Phi}_m$ gives the total potential increase along the field line.

[42] We now use this approach to approximate the potential in the FAST data given by *Carlson et al.* [1998, Figure 2].

This is taken at an altitude of around 3965 km, which we denote by ℓ_{FAST} . The current density at this altitude, j_{FAST} , varies from 1 to 2.5 μAm^{-2} , so we consider both of these cases. We use the current continuity condition in equation (9) to obtain corresponding values for j_m , which are 4.29 (case 1) and 10.7 (case 2) μAm^{-2} . These are high current densities, so this is a strong downward current event. We take typical ionospheric and magnetospheric electron temperatures of 1 eV and 1 keV, giving $\eta = 10^{-3}$; n_m is taken to be 10^{11} m^{-3} , slightly lower than used previously to account for the fact that this event occurred at night, giving $n_m/n_0 = 10^5$; finally, the ion scale height is taken to be 150 km, slightly larger than before to account for transverse ion heating effects which modify the distribution of ions. The results are shown in Figure 6; the total potential increase is 1730 V for

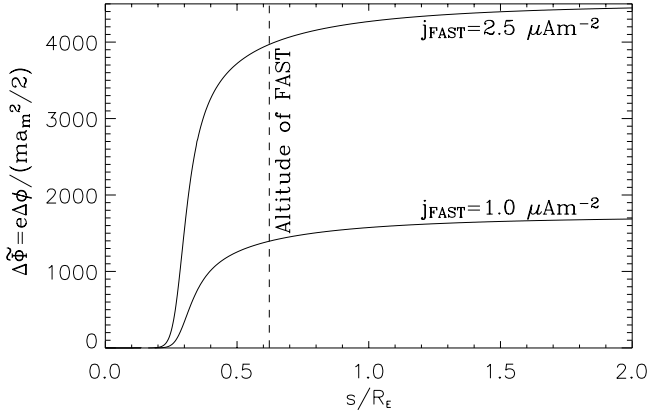


Figure 6. Comparison with data given by *Carlson et al.* [1998, Figure 2]. Taking $j_m = 4.29$ and $10.7 \mu\text{Am}^{-2}$ gives current densities at FAST of 1 and $2.5 \mu\text{Am}^{-2}$, respectively. Taking $\eta = 10^{-3}$, an ionospheric temperature of 1 eV, $n_m/n_0 = 10^5$ and $h = 150$ km, we obtain $\Delta\Phi_{FAST}$ values of 1400 and 3970 V for each case, which correspond well with the bottom panel of their figure.

case 1, and 4510 V for case 2. Most of the acceleration has taken place by ℓ_{FAST} giving $\Delta\phi_{FAST} = 1400$ V for case 1, and 3970 V for case 2. These values show excellent agreement with the bottom panel of *Carlson et al.* [1998, Figure 2], where ϕ_{FAST} was inferred from $\int \mathbf{E} \cdot d\mathbf{s}$ along the satellite trajectory. The potential in Figure 2 of *Carlson et al.* [1998] varies from ~ 1 to ~ 4 kV.

[43] The Taylor series expansions can be used for this example, where the B/n peak lies at 2200 km, and $c_p = 3.89 \times 10^4$.

[44] In case 1, $j_{FAST} = 1 \mu\text{Am}^{-2}$, giving $\alpha = 4.51 \times 10^{-4}$ and $\Psi = 0.675 < 1$. Thus we use the expansion in equation (35) to give $\tilde{\Phi}_m \approx -1730$, which is accurate to 0.8%.

[45] In case 2, $j_{FAST} = 2.5 \mu\text{Am}^{-2}$, giving $\alpha = 1.13 \times 10^{-3}$ and $\Psi = 1.25$. Since this value is around 1, either expansion should give a good approximation. From equation (35), we obtain $\tilde{\Phi}_m = -4220$ eV, accurate to 6.4%; equation (40) yields $\tilde{\Phi}_m = -4270$ eV, accurate to 5.2%. This illustrates that both approximations still work well in the region $\Psi \approx 1$.

5. Dimensional Expressions

[46] While it is useful to work in terms of dimensionless quantities (α , η and $\Delta\tilde{\Phi}$) to obtain expressions for $\tilde{\Phi}_m$, the total normalized potential increase along the field line, it can be informative to return to dimensional quantities in order to gain further physical insight. Substituting equations (10) and (11) into the small- Ψ expression for $\tilde{\Phi}_m$ in equation (35), noting that $\tilde{\Phi}_m = 2e\phi_m/ma_m^2$ and $\phi(\ell_0) = 0$, we obtain:

$$-\phi_m = \frac{3}{2} \left(\frac{m^{1/2} j_m B_p k T}{e^{5/2} n_p B_m} \right)^{2/3} + \frac{1}{2} \left(\frac{m^2 j_m^4 B_p^4 k T}{e^7 n_p^4 B_m^4} \right)^{1/3} + \frac{m}{6e^3} \frac{j_m^2 B_p^2}{n_p^2 B_m^2} \quad (41)$$

[47] We can obtain a similar expression for $\tilde{\Phi}_m$ for large Ψ using equation (40):

$$-\phi_m = \frac{kT}{e} \ln \left(\frac{j_m^2 B_p^2}{n_p^2 e^2 B_m^2} \frac{m}{kT} \right) + \frac{m}{2e^3} \frac{j_m^2 B_p^2}{n_p^2 B_m^2} + \frac{kT}{e} \quad (42)$$

[48] It is interesting to note that both of these expressions for ϕ_m are independent of the ionospheric temperature, a_m , and ionospheric electron number density, n_m . This highlights the fact that the precise properties of the ionosphere are unimportant to the acceleration of the field-aligned electrons: the ionosphere is simply the reservoir from which the necessary electrons are extracted.

5.1. Potential Drop in Terms of Speeds

[49] We can derive expressions for ϕ_m , the actual potential increase along the field line, in terms of two characteristic speeds: the mean electron drift speed at the B/n peak, u_p , defined as

$$u_p = \frac{j_p}{n_p e} \quad (43)$$

where $j_p = j_m B_p / B_m$, and the magnetospheric thermal velocity, v_{th} , given by

$$v_{th}^2 = \frac{2kT}{m} \quad (44)$$

[50] If we substitute equations (43) and (44) into equation (29), we find that

$$\Psi^3 = \left(\frac{u_p}{v_{th}} \right)^2 \quad (45)$$

[51] Thus the small- Ψ expression for $\tilde{\Phi}_m$ in equation (35) corresponds to cases where $u_p \ll v_{th}$, i.e., for relatively small current densities and moderate to high magnetospheric electron temperatures. We substitute equations (43) and (44) into (41) to obtain an expression for ϕ_m in this regime:

$$-\phi_m = \frac{m}{2e} \left(3 \left(\frac{u_p}{v_{th}} \right)^{2/3} v_{th}^{4/3} + \frac{u_p^{4/3} v_{th}^{2/3}}{2^{1/3}} + \frac{u_p^2}{3} \right) \quad (46)$$

[52] In the alternative regime, where $\Psi > 1$ or $u_p \gg v_{th}$, implying higher current densities and lower magnetospheric electron temperatures, we substitute equations (43) and (44) into (42) to obtain:

$$-\phi_m = \frac{m}{2e} \left(v_{th}^2 \ln \left(2 \frac{u_p^2}{v_{th}^2} \right) + u_p^2 + v_{th}^2 \right) \quad (47)$$

5.2. Potential Drop in Terms of Current Densities

[53] Alternatively, we can derive $\tilde{\Phi}_m$ in terms of two characteristic current densities: the beam current density at the B/n peak, written using equation (9) as

$$j_p = j_m \frac{B_p}{B_m} \quad (48)$$

and the field-aligned thermal current density, j_{th} , due to the downgoing component of the Maxwellian electron distribution (i.e., $0 < v_{\parallel} < \infty$, $0 < v_{\perp} < \infty$) at ℓ_0 :

$$\begin{aligned} j_{th} &= -e \int_0^{\infty} v_{\parallel} f_M dv_{\parallel} \int_0^{\infty} (2\pi v_{\perp}) dv_{\perp} \\ &= -en_0 \sqrt{\frac{kT}{2\pi m}} \end{aligned} \quad (49)$$

where

$$f_M = n_0 \left(\frac{m}{2\pi kT} \right)^{\frac{3}{2}} \exp \left(-\frac{1}{kT} \left(\frac{m}{2} (v_{\parallel}^2 + v_{\perp}^2) - e\phi \right) \right) \quad (50)$$

[54] Of course, we assume that these electrons mirror, so this population does not carry a net current. The parameter Ψ in equation (29) can now be written as

$$\Psi^3 = \frac{1}{4\pi} \frac{j_p^2}{j_{th}^2} \frac{n_0^2}{n_p^2}, \quad (51)$$

[55] So, the small- Ψ expression (41), valid when $j_p \ll |j_{th}|$, can be written in terms of (48) and (49) to give

$$\begin{aligned} -\phi_m &= \frac{m}{2e^3} \left(3 \left(\frac{2\pi}{n_0^2 n_p} \right)^{2/3} j_p^{2/3} |j_{th}|^{4/3} \right. \\ &\quad \left. + \left(\frac{2\pi}{n_0^2 n_p^4} \right)^{1/3} j_p^{4/3} |j_{th}|^{2/3} + \frac{j_p^2}{3n_p^2} \right) \end{aligned} \quad (52)$$

[56] Similarly, the large- Ψ expression in equation (42), valid when $|j_{th}| \ll j_p$, can be written as

$$-\phi_m = \frac{m}{e^3} \left(\frac{2\pi j_{th}^2}{n_0^2} \ln \left(\frac{j_p^2}{j_{th}^2} \frac{n_0^2}{2\pi n_p^2} \right) + \frac{j_p^2}{2n_p^2} + \frac{2\pi j_{th}^2}{n_0^2} \right) \quad (53)$$

[57] Further simplifications can be made to equations (52) and (53) by noting that $n_p \approx n_0$.

6. Discussion and Conclusions

[58] The analysis presented here reveals that the B/n peak is central to the solution of the downward current region. Mathematically, the equations contain a stationary point which lies slightly beyond the B/n peak. Examination of this stationary point yields a near-exact solution for $\tilde{\Phi}_m$, the total potential increase along the field line (given the model parameters, and n_q and B_q). Taylor series expansions of the exact solution can be carried out to give two simplified nonlinear current-voltage relations. Since the stationary point is so close to the B/n peak, approximations can be derived for which we use the number density and magnetic field strength at the B/n peak. One approximation is valid for lower current densities and moderate to high magnetospheric temperatures (~ 1 keV), while the other takes over for higher current densities and lower magnetospheric temperatures. Typically, the first expansion will be more useful for most downward current regions in the Earth's magnetosphere, except for stronger events with particularly high current densities. Both of these expansions, when

written in dimensional form, are independent of ionospheric equilibrium parameters, illustrating that the exact properties of the ionosphere are unimportant in this model.

[59] Observations suggest that acceleration in the downward current region can occur over a very small distance [Ergun *et al.*, 2003] (i.e., a double layer). In this case, the change in potential along the field line is compacted, which can be achieved via a sharp decrease or change in ion number density at a certain altitude [Temerin and Carlson, 1998]. Just as Knight's [1973] model of the upward current provides a good overview of the region as a whole, neglecting double layers, we describe the downward current region on a similarly large scale. Thus we find a smooth transition in potential, but it is quite possible that this overall change is confined to sharp increases in potential contained within several double layers [Andersson *et al.*, 2002]. In any case, the overall change in potential is likely to be similar in both cases. In paper 1, we find that it is the properties of the small region surrounding the B/n peak (containing the stationary point ℓ_q) which solely determine the total potential change $\tilde{\Phi}_m$. This has been corroborated by the analytical work presented here, which shows that we can determine $\tilde{\Phi}_m$ simply by solving the stationary point equations at ℓ_q . If we were to include ion motion in this model, it is possible that the ion distribution would steepen into a double layer, which would preserve the single B/n peak and effectively move ℓ_q even closer to it: thus our analysis should still be appropriate.

[60] The location of the B/n peak is principally dependent upon the ion scale height and number density, n_m/n_0 . In Cattell *et al.*'s [2004] statistical survey of the occurrence of upward accelerated electron beams, many more beams were observed on field lines where the ionospheric foot point is in darkness than when it is illuminated. This makes sense in terms of the model, since at night time, the number density and scale height will be smaller because of lack of photoionization and cooler temperatures. These two factors cause the B/n peak, and hence the stationary point, to move earthward. With a smaller number density, the ionosphere will provide fewer charge carriers which, on encountering lower ion number densities due to the decreased scale height, will need to be accelerated at lower altitudes to meet the demands of quasineutrality and carry the required current.

[61] The current-voltage relations derived here show good agreement with observational data. Qualitatively, our model predicts potential increases of ~ 100 V to ~ 1 kV, which tally well with observations of downward current regions. Quantitatively, our model agrees very well with the FAST data from Carlson *et al.* [1998]. It will be desirable to make further comparisons with data to check consistency over a range of current densities.

[62] **Acknowledgments.** Alexandra Cran-McGreehin is supported by the Carnegie Trust for the Universities of Scotland. The authors wish to thank the referees for their comments.

[63] Shadia Rifai Habbal thanks Goran T. Marklund, Michael A. Temerin, and another referee for their assistance in evaluating this paper.

References

Andersson, L., R. E. Ergun, D. L. Newman, J. P. McFadden, C. W. Carlson, and Y.-J. Su (2002), Characteristics of parallel electric fields in the downward current region of the aurora, *Phys. Plasmas*, *9*, 3600.

- Carlson, C. W., J. P. McFadden, R. E. Ergun, M. Temerin, W. Peria, F. S. Mozer, D. M. Klumppar, E. G. Shelley, C. Cattell, and R. Pfaff (1998), FAST observations in the downward auroral current region: Energetic upgoing electron beams, parallel electric fields, and ion heating, *Geophys. Res. Lett.*, *25*, 2017.
- Cattell, C., J. Dombeck, W. Yusof, C. Carlson, and J. McFadden (2004), FAST observations of the solar illumination dependence of upflowing electron beams in the auroral zone, *J. Geophys. Res.*, *109*, A02209, doi:10.1029/2003JA010075.
- Cran-McGreehin, A. P., and A. N. Wright (2005), Electron acceleration in downward auroral field-aligned currents, *J. Geophys. Res.*, *110*, A10S15, doi:10.1029/2004JA010898.
- Elphic, R., J. Bonnell, R. J. Strangeway, C. W. Carlson, M. Temerin, J. P. McFadden, R. E. Ergun, and W. Peria (2000), FAST observations of upward accelerated electron beams and the downward field-aligned current region, in *Magnetospheric Current Systems*, *Geophys. Monogr. Ser.*, vol. 118, edited by S. Ohtani et al., p. 173, AGU, Washington, D. C.
- Ergun, R. E., et al. (1998), FAST satellite observations of electric field structures in the auroral zone, *Geophys. Res. Lett.*, *25*, 2025.
- Ergun, R. E., L. Andersson, C. W. Carlson, D. L. Newman, and M. V. Goldman (2003), Double layers in the downward current region of the aurora, *Nonlinear Processes Geophys.*, *10*, 45.
- Jasperse, J. (1998), Ion heating, electron acceleration, and the self-consistent parallel electric field in downward current regions, *Geophys. Res. Lett.*, *25*, 3485.
- Knight, S. (1973), Parallel electric fields, *Planet. Space Sci.*, *21*, 741.
- Marklund, G., L. Blomberg, C.-G. Fälthammar, and P. A. Lindqvist (1994), On intense diverging electric fields associated with black aurora, *Geophys. Res. Lett.*, *21*, 1859.
- Rönnmark, K. (2002), The auroral current-voltage relation, *J. Geophys. Res.*, *107*(A12), 1430, doi:10.1029/2002JA009294.
- Salas, S., E. Hille, and G. Etgen (2003), *Calculus: One and Several Variables*, 9th ed., John Wiley, Hoboken, N. J.
- Temerin, M., and C. W. Carlson (1998), Current-voltage relationship in the downward current region, *Geophys. Res. Lett.*, *25*, 2365.
- Vedin, J., and K. Rönnmark (2004), A linear auroral current-voltage relation in fluid theory, *Ann. Geophys.*, *22*, 1719.
- Wright, A. N., and A. W. Hood (2003), Field-aligned electron acceleration in Alfvén waves, *J. Geophys. Res.*, *107*(A3), 1135, doi:10.1029/2002JA009551.

A. P. Cran-McGreehin and A. N. Wright, Mathematical Institute, University of St. Andrews, St. Andrews, Fife KY16 9SS, UK. (alex@mcs.st-and.ac.uk; andy@mcs.st-and.ac.uk)